CrossMark
click for updates

Predicted structural evolution and detailed insight into configuration correlation, mechanical properties of silicon–boron binary compounds†

Bo Zhang,[a] Lailei Wu[b] and Zhihong Li*[a]

The crystal structures, phase stability, mechanical and electronic structures of silicon–boron binaries have been investigated systematically using first-principles of pseudopotential calculations. The calculated formation enthalpies of α-SiB_3, SiB_6 and SiB_n follow the sequence: ΔH_f (α-SiB_3) > ΔH_f (SiB_6) > ΔH_f (SiB_n), which is in good agreement with the previous experimental results. Monoclinic SiB_6 with $P2_1/m$ symmetry and hexagonal SiB_{36} with a B_{80} unit (a ring linked by diametrically located $2 \times B_{28}$, $2 \times B_{12}$) are suggested as the more energetically and mechanically favorable phases by our calculations. The predicted bulk modulus of Si–B binaries is between 120 and 180 GPa, while there is a dramatic drop for two kinds of α-SiB_3 in the shear modulus from 130.3 GPa (SiB_3) to 71.1 GPa (SiB_4). We infer that the additional centered boron atoms, located long the spatial diagonal in SiB_4, is responsible for the weakness along this direction. In addition to β-SiB_3, the new proposed $P2_1/m$-SiB_6 and $R3m$-SiB_6 is found to be semiconducting with 0.41 eV indirect and 1.654 eV direct band gap, respectively. There is no band gap provided by band structures of SiB_4 and SiB_{36}, as well as their DOS values are quite large at Fermi level, indicating they are energetically unstable under 0 K and GPa.

1. Introduction

Boron-rich borides are classical refractory materials: light-weight, extremely hard, and exceptionally thermal stability.[1,2] Even more importantly, boron-rich compounds have attracted extensive attention for their high melting-points, semi-metallic/metallic, ascending Seebeck coefficients and electrical conductivities with increasing temperature.[3–5] Excellent electrical conductivity combined with weak thermal conductivity contributes to generate good thermoelectric properties in borides. In particular the silicon borides, possessing extremely higher chemical and thermal stabilities, have great potential for thermoelectric materials in extreme conditions (high-temperature, strong chemical corrosion, etc.).[6,7] After reviewing the whole Si–B system, there are mainly three kinds of binary compounds, usually referred to as SiB_3, SiB_6 and SiB_n. To be precise, "SiB_3" is the stoichiometry designation for Si–B compounds ranging from $SiB_{2.8}$ to SiB_4.[8–15] This range is taken as an indication of a wide homogeneity phase region for a solid with the SiB_3 structure. Another probable confusion should be

noticed that SiB_3 here is more accurately α-SiB_3, since an orthorhombic phase, termed β-SiB_3, has been obtained in gallium flux conditions at lower temperatures by J. R. Salvador et al.[16] Unless otherwise noted, α-SiB_3 is used in this paper to designate the phase with that kind of crystal structure and not to indicate a specific composition. Usually, α-SiB_3 is synthesized by melting a mixture of boron (5–10 weight%) and silicon in a furnace, however, it is barely possible to obtain it purely, always being accompanied with SiB_6 products.[8–11,13,14] α-SiB_3 has the same structure as boron carbide (B_4C or $B_{12}C_2$), and other borides belonging to a class of icosahedral boron-rich solids that includes α-rhombohedral (α-rh) boron.[7,17,18] In 1956, Zhuravlev firstly found that SiB_6 was a cubic phase through the X-ray structure analysis.[19] Another different structure of SiB_6 was determined by M. Vlasse using single-crystal X-ray diffraction,[20] it has a complex crystal structure with about 43 silicon atoms and 238 boron atoms in its orthorhombic unit cell, containing interconnected icosahedra, icosihexahedra, as well as several isolated boron and silicon atoms. Similar to α-SiB_3, the ratio of B/Si = 6/1 is stoichiometry approximation for the Si–B binaries ranging from $SiB_{5.7}$ to $SiB_{6.1}$ contributed by inter-changing silicon and boron atoms within the multiple sites.[17,20] SiB_n is obtained through the peritectic reaction: liquid + β-boron solid solution = SiB_n at 2293 K,[6] and was first synthesized by Giese et al., known as SiB_{14}.[21] However, the value width of n has been a controversy so far that previous study claimed that n ranges from 16 to 26;[22] ten years later, T. B. Massalski et al. enlarged the n values to the limits between 13.9 and 32.3;[23] after

[a] Key Laboratory of Advanced Ceramics and Machining Technology of Ministry of Education, School of Materials Science and Engineering, Tianjin University, Tianjin 300072, China. E-mail: lizhihong@tju.edu.cn; Tel: +86 22 27404260

[b] Key Laboratory of Metastable Materials Science and Technology, College of Material Science and Engineering, Yanshan University, Qinhuangdao 066004, China

another decade, a wider value range of n was introduced by Y. Imai *et al.*[7] that the Si-rich solubility limit at 1873 K is 5.4 at%, corresponding to $SiB_{17.5}$, and the probable maximum value of n reached up to 60.

First-principles calculation is a valuable prediction approach to understand crystal parameters, thermodynamic properties and studying their structural transformations.[7,24,25] Band calculations of electronic densities of states and total energies of the Si–B system have been attempted by Y. Imai[7] using first-principles pseudopotential method within local density approximation. The theoretical achievements about Si–B compounds were reviewed by B. Albert and H. Hillebrecht,[25] crystal structures of this system and the structural features between the specific Si–B compounds and their structurally related borides were summarized and sorted. β-Rhombohedral boron (β-rh B) has been an attractive topic of calculation researches for decades.[24–29] The crystal structure, thermodynamic stability, specific heat and electronic structure of β-rh B were introduced by T. Ogitsu *et al.*[24] including experimental and theoretical calculation efforts. Shang *et al.*[29] considered that β-rh B obtained several different atomic densities: 105–110 atoms per rhombohedral cell through examining the total energy of β-rh B as a function of atomic density. For the tetragonal configuration of boron,[30–36] the crystal and electronic structures of α-tetragonal (α-t or I-t) B (B_{50}, 50 atoms per cell) were investigated by Hayami and Otani[31] from first-principles, while the other unstable β-tetragonal (β-t or II-t) B is probably obtained through nonequilibrium growth based on the research of surface energy and crystal growth.[35] α-rh B (B_{12}), the significant basic icosahedral boron unit, has also been focused by researchers employing means of first-principles calculations,[29,36–38] and it is shown that α-rh B is a semiconductor with an indirect band gap of 1.70 eV in the study of D. Li *et al.*[36] The majority of the research emphases were about the structures and properties of the elementary boron, and thermodynamic properties of the Si–B compounds. However, to our knowledge, there are no comparative investigations on the mechanical properties and underlying relations between the phases of Si–B system. Therefore, using means of first-principles calculations based on density functional theory, in this paper, we report the enthalpies of formation, elastic constants and electron structures of the Si–B system and other related phases: α-SiB_3 (SiB_3, SiB_4), β-SiB_3, SiB_6, SiB_{36}. The relevant data of α-rhombohedral boron (α-rh B), β-rhombohedral boron (β-rh B), α-tetragonal boron (α-t B), and γ-B_{28} (high pressure phases) are also available in ESI† for comparison and comprehensive understanding.

2. Computational details

First-principles calculations were performed using CASTEP code based on Density Functional Theory (DFT).[39] The exchange and correlation functions were treated by generalized gradient approximation with the parameterization by Perdew–Burke–Ernzerhof (GGA-PBE).[40,41] The electronic configurations of each element were $2s^2 2p^1$ for B and $3s^2 3p^2$ for Si, respectively. The mass of B atom is 10.81 and Si atom is 28.085. The oxidation state of any atom is 0, and none temperature factors were set on atoms. The convergence of calculations was initially checked by a $5 \times 10 \times 10$ k-point and cutoff energy of 310 eV. The ground state and elastic constants (C_{ij}) of all considered Si–B phases are then calculated for each fully relaxed structure. Bulk and shear moduli were estimated based on Voight–Reuss–Hill (VRH) approximation.[42] Elastic moduli (E) and Poisson's ratio (ν) were obtained based on the relationship: $E = 9BG/(3B + G)$, $\nu = (3B - 2G)/(6B + 2G)$. The universal elastic anisotropy index (A^U)[43] is obtained from the B and G of Voigt and Reuss with the equation: $A^U = 5G_V/G_R + B_V/B_R - 6$.

3. Results and discussions

3.1. Structural stability

Mechanical stability, a necessary condition for a stable phase to exist in experiments, was firstly checked for all of the Si–B system crystals according to the Born–Huang criterion.[44,45] If all the individual elastic moduli of a specific phase are satisfied, the mechanical stability criteria indicate its stability. The calculated elastic constants of Si–B system phases are listed in Table 1, and it can be found that α-SiB_3 (SiB_3, SiB_4), β-SiB_3 and SiB_{36} satisfy the Born–Huang criterion, indicating their mechanical stabilities. However, cubic $Pm\bar{3}m$-SiB_6 (ref. 19) ($C_{44} = -4.13$ GPa) is mechanically unstable. To get a further understanding of the structural configuration of SiB_6, we have employed the in-house developed CALYPSO[46,47] structure prediction methodology to conduct the structure search for SiB_6. Our search identified 20 stable structures: SiB_6-01_01, SiB_6-02_01,…, SiB_6-19_01, SiB_6-20_01. Monoclinic $P2_1/m$-type (space group number: 11) SiB_6-01_01 with the lowest energy is founded to be the most energetically favorable among the 20 configurations, calculated energy of these 20 structures are available in the ESI.† Hexagonal $R3m$-type (space group number: 160) SiB_6-08_01 is also considered in this study because of its special structure (it will be discussed in the following sections). For convenience, SiB_6-01_01 denotes as SiB_6 and SiB_6-08_01 is abbreviated as SiB_6-81. According to Table 1, monoclinic $P2_1/m$-SiB_6 and hexagonal $R3m$-SiB_6-81 are qualified for mechanical stability. To furtherly prove the reliability of the new suggested structure of SiB_6, the XRD pattern was calculated. As shown in Fig. 1, it can be found that our theoretical results are in generally accordance with the experimental XRD data[17,48,49] in consideration of only isolated data provided from the previous work,[48] which the XRD peaks of Si, SiB_3 and other Si–B compounds have been eliminated from based on available reports.[17,49]

To verify the thermodynamic stability of the considered phases in the Si–B system, the formation enthalpies (ΔH_f) are calculated as listed in Table 2 and compared with available experimental results.[22,50] The formation enthalpy of $Si_x B_y$ phase can be defined as

$$\Delta H_f = E_{total}(Si_x B_y) - (x E_{total}(Si) + y E_{total}(B)) \tag{1}$$

where $E_{total}(Si_x B_y)$ is the total energy of $Si_x B_y$ at equilibrium lattice constants; $E_{total}(Si)$ and $E_{total}(B)$ are the calculated total energy of Si (-101.901 eV) and B (-70.488 eV), x and y ($x + y = 1$)

Table 1 Calculated elastic constants C_{ij} (in GPa) of considered Si–B phases

Phase	S.G.	C_{11}	C_{22}	C_{33}	C_{44}	C_{55}	C_{66}	C_{12}	C_{13}	C_{14}
SiB$_3$	$R\bar{3}m$	326.0		349.3	144.0			86.3	92.1	−2.47
SiB$_4$	$R\bar{3}m$	259.0		373.5	51.7			125.8	104.3	−37.9
SiB$_6$	$Pm\bar{3}m$	402.6			−4.13			19.31		
	$P2_1/m$	373.6	351.6	432.5	127.2	176.4	174.8	101.5	101.4	
		29.5(C_{23})		16.0(C_{15})		−5.8(C_{25})		−23.7(C_{35})		−20.5(C_{46})
SiB$_6$-81	$R3m$	187.8		196.1	117.3			74.0	93.3	74.9
SiB$_{36}$	$R3m$	419.3		431.5	146.8			72.9	75.6	36.7
β-SiB$_3$	$Imma$	288.8	369.6	357.4	123.3	134.6	130.8	51.5	64.3	
		72.6(C_{23})								
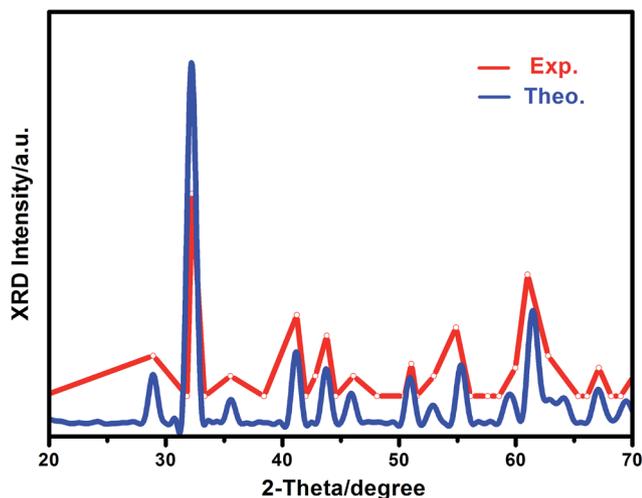
Fig. 1 Calculated X-ray diffraction pattern of $P2_1/m$-SiB$_6$ compared with experimental data.

are the atomic fractions of Si and B, respectively. According to Table 2, it can be observed that our calculated formation enthalpies of Si–B phases generally agree with the experimental results in the previous reports.[22,48] Taking α-SiB$_3$ (SiB$_3$, SiB$_4$), SiB$_6$ and SiB$_{36}$ (SiB$_n$) for comparison, SiB$_{36}$ (SiB$_n$) has the most negative ΔH_f (−2.883 eV per atom) and the formation enthalpies of the three kinds of compounds follow the sequence of ΔH_f (α-SiB$_3$) > ΔH_f (SiB$_6$) > ΔH_f (SiB$_n$). Consequently, our calculated results are in good agreement with the previous experimental data,[51] that SiB$_n$ has the highest stable temperature (about 2200

K) and the lowest (about 1400 K) is for α-SiB$_3$. For SiB$_3$ and SiB$_4$, they present little difference in the formation enthalpies, since these two binaries share similar structure belonging to α-SiB$_3$ phase. It can also be furtherly determined that $P2_1/m$-SiB$_6$ is more energetically favorable than $Pm\bar{3}m$-SiB$_6$ and SiB$_6$-81, since ΔH_f of the former one is less than the latter ones. α-SiB$_3$ (SiB$_3$, SiB$_4$) and γ-B$_{28}$ is structurally related to α-rh B, from Table 2 and ESI,† it can be found that α-rh B is the most thermodynamic stable phase of those related structures and it is naturally interpreted as foreign atoms (Si atoms) disturbing the original charge distribution, thus more energy being needed to maintain equilibrium of the crystal system. However, the ΔH_f of SiB$_{36}$ whose structure is based on the framework of β-rh B is much more negative than β-rh B. Different from the previous condition, introducing Si atoms to the complicated polyatomic β-rh B crystal is helpful to reduce internal energy of the structure. The rigorous synthesis and stability conditions, that β-SiB$_3$ needs producing from a lower temperature reaction (1000–850 °C) in metallic flux to permit the total bypass of the compound α-SiB$_3$,[16] indicate the highest ΔH_f of β-SiB$_3$ in Table 2.

The calculated structural parameters and Wyckoff positions of different crystals, after full stress and position relaxation, are shown in Table 3 and ESI.† In general, our results are in good accordance with previous theoretical and experimental results as shown in Table 3.[9,11,16,19,52]

As shown in Fig. 2, B$_{12}$ icosahedra, as the single primary unit of α-rh B, is an indispensable structural element for most of the Si–B compounds. It can be found that SiB$_3$ (Fig. 2a) and SiB$_4$ (Fig. 2b) are established with B$_{12}$ icosahedra as the framework. The B$_{12}$ units are situated on the corners of a rhombohedron

Table 2 Calculated formation enthalpies of Si–B system compared with available experimental results

Phase	S.G.	ΔH_f (eV per atom)	ΔH_f (kJ per mol per atom)	ΔH_f (Exp.) (kJ per mol per atom)
SiB$_3$	Hex.($R\bar{3}m$)	−1.196	−115.449	−109.4 (ref. 48)
SiB$_4$	Hex.($R\bar{3}m$)	−1.133	−109.336	−109.4 (ref. 48)
SiB$_6$	Cub.($Pm\bar{3}m$)	−1.218	−117.486	−148.3[48],
	Mon.($P2_1/m$)	−1.267	−122.233	−121[22]
SiB$_6$-81	Hex.($R3m$)	−1.248	−120.458	
SiB$_{36}$	Hex.($R\bar{3}m$)	−2.883	−278.161	
β-SiB$_3$	Ort.($Imma$)	−0.0699	−6.746	

Table 3 Calculated and experimental lattice parameters of considered Si−B phases

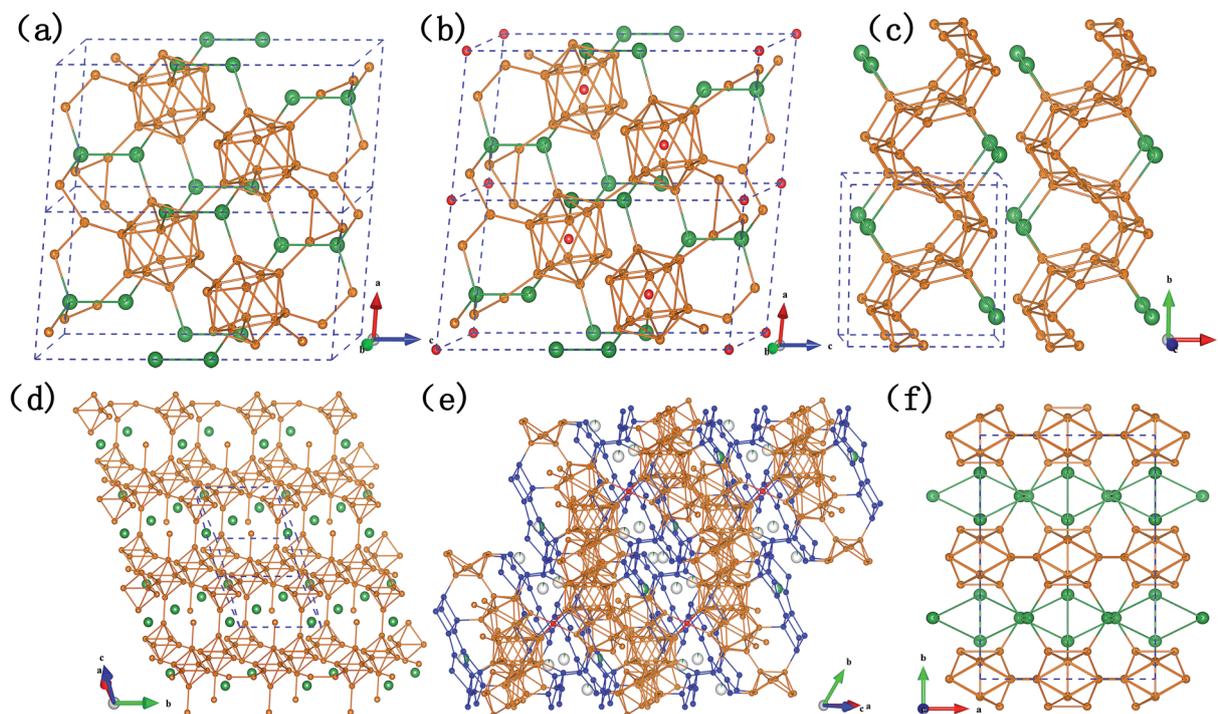| Phase	Structure	Lattice parameter (Å)					
		Theory (this work)			Experiment (ref.)		
		a	b	c	a	b	c
SiB_3	Hex.($R\bar{3}m$)	6.319	6.319	12.71	6.32	6.32	12.71 (ref. 11)
SiB_4	Hex.($R\bar{3}m$)	6.319	6.319	12.71	6.33	6.33	12.74 (ref. 9)
SiB_6	Cub.($Pm\bar{3}m$)	4.13	4.13	4.13	4.13	4.13	4.13 (ref. 19)
	Mon.($P2_1/m$)	6.26 ($\beta = 90.03°$)	6.22	3.07			
SiB_6-81	Hex.($R3m$)	5.85	5.85	7.48			
SiB_{36}	Hex.($R\bar{3}m$)	11.01	11.01	23.90	10.98	10.98	23.86 (ref. 51)
β-SiB_3	Ort.($Imma$)	8.39	12.57	6.21	8.39	12.57	6.21 (ref. 16)

Fig. 2 Crystal structures of six Si−B compounds after full stress and position relaxation. (a) SiB_3; (b) SiB_4; (c) $P2_1/m$-SiB_6; (d) SiB_6-81; (e) SiB_{36}; (f) β-SiB_3. Boron and silicon atoms are marked as brown and green, respectively; boron atoms in special positions of their structures were marked as red in (d) (e), respectively; boron bilayers were displayed in blue color in (e) SiB_{36}.

just as in α-rh B (two 18h sites in hexagonal arrangement), Si atoms are located on the spatial diagonal of the rhombohedron and link three icosahedra each of one layer (6c site), as a result, the remaining valence electron of Si atom contribute to bonding a pair of close Si atoms to form a Si_2 group. Thus, the 2e3c boron bonds (B–B distance: 1.67 Å) in α-rh B are replaced by 2e2c silicon bonds (Si–Si distance: 2.39 Å for SiB_3 and 2.29 Å for SiB_4), causing a distinct reduction of the c/a ratio (12.56/4.908 for α-rh B in hexagonal arrangement). Overall, it is the partial incorporation, which results from silicon atoms going into the polar position of the icosahedron, that leads to the high silicon content and the relatively large lattice parameters.

The remarkable difference between SiB_3 and SiB_4 is that there is an additional B atom (3a site) in SiB_4 lattice located in the

center of each icosahedron, accordingly, which induce slight variations of the bond lengths of inter- and intra-icosahedral boron atoms. However, such little change did not affect the lattice parameters in our calculated results (as shown in Table 3). It also can be explained that in α-SiB_3, some Si atoms are randomly distributed in the B_{12} cages resulting in very distorted icosahedra,[18] according to different situation of inside Si atoms of B_{12}-cages in these two α-SiB_3 phases. In contrast, Si atoms in β-SiB_3 are rigorously excluded from the cages (as shown in Fig. 2f), thus resulting in more regular icosahedra. It was even considered as the first Si–B binary phase that is fully crystallographically ordered without any Si/B mixed sites or disorder.[16]

The structures of two SiB_6 compounds are quite different. In Fig. 2d, the hexagonal crystal ($R3m$-SiB_6-81) belongs to layered-

like structure based on the B_6 octahedron unit composed of eight boron atoms, and with silicon atoms located in interstitial spaces; however, configuration of the monoclinic one ($P2_1/m$-SiB_6) is built on zig-zag networks bonded by boron atoms in Fig. 2c.

Comparing the Si–B binaries (Fig. 2a–f), it can be noticed that the structures bonded with boron atoms become more and more complex along with the increasing content of boron. For example, B_{28} triply fused icosahedra (three condensed icosahedra in Fig. 2e) were formed in SiB_{36} by 28 boron atoms in addition to B_{12} icosahedra-the only polyhedron in α-SiB_3. Si atoms partially occupy the interstitial sites between the polyhedrons in SiB_{36} instead of being located in the 6c sites completely in α-SiB_3. With regard to the structural influence on the B–B bond lengths of inter- and intra-icosahedra, we find that the distances are all beyond 1.85 Å in the B_{12} units of two α-SiB_3 structures, while they reduce to around 1.70 Å in SiB_{36}.

As the last two phases in the boron-rich end of the Si–B phase diagram, SiB_{36} and β-rh B have a similar formation based on B_{28} triply fused icosahedra as the boron framework. Differing to previous structures of SiB_{36} (ref. 25 and 53) those could be analogized as β-rh B framework with interstitial sites between polyhedrons and B atoms in icosahedra partly occupied by Si atoms, however, in this work there is a new found boron B_6 unit comprised with 6 boron atoms. To be specific, as highlighted by blue atoms in Fig. 2e, two quadrilateral-B_4 connect with each other by a shared B–B bond (B_7–B_9, bond length: 1.79 Å) producing two included angle: 121.62° and 115.64°. The linked B_6 units together with B atoms of B_{28} units form a layer being vertical to the spatial diagonal. There are four kinds of boron positions in a B_6 unit, B_1: bonded with two neighbor B atoms of its own B_6 unit and a B atom of the neighbor B_6 unit in the same layer; B_2: bonded with one B atom of B_{28} unit, one of the neighbor parallel layer, in addition to two intra-B_6 unit B–B bonds; B_7: three intra-B_6 unit B–B bonds and a B–B bond with a B atom in a icosahedron; B_9: similar to B_7 except the bond with icosahedral atom, however, linked with a B atom of B_{28} unit. The lengths of B–B bond intra-B_6 unit are B_1–B_2: 1.71 Å, B_2–B_7: 1.79 Å, B_1–B_9: 1.82 Å, B_7–B_9: 1.79 Å, respectively. The bond lengths of between intra- and inter-B_6 unit are layer–layer: B_2–B_2 = 1.78 Å, intra-B_6 with B_{28}: B_9–B_{10} = 1.69 Å and B_2–B_3 = 1.73 Å, intra-B_6 with B_{12}: B_7–B_5 = 1.67 Å.

From Fig. 2e and 3, we can find that two layers constituted with B_{80} units (B_{80}, a ring linked by diametrically located 2 × B_{28}, 2 × B_{12}) are connected by two neighbor parallel B_6 layers, in addition to be covalently bound through junctional atom B_{15} (highlighted as red atoms in Fig. 2e). Therefore, it can be considered as B_{80} layers and B_6 layers being stacked vertically to the spatial diagonal make the framework of SiB_{36}, and Si atoms are partially located at interstitial sites in the space surrounded by the joint B_6 layers.

3.2. Elastic properties

The calculated individual elastic constants within the strain–stress method are listed in Table 1 for considered Si–B system crystals. In general, all of the mechanically stable phases show
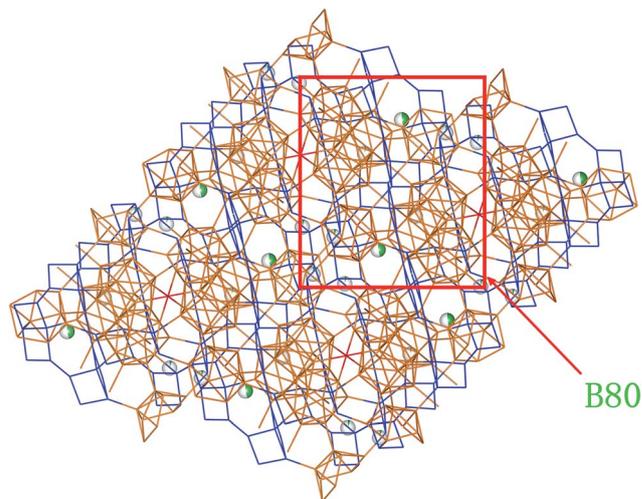

Fig. 3 B_{80} unit (a ring linked by diametrically located 2 × B_{28} and 2 × B_{12}) in SiB_{36}.

the considerably higher values of C_{11}, C_{22} and C_{33} than that of C_{44}, indicating relatively higher incompressibility along a-, b- and c-axis. Furthermore, among all the individual elastic constants, C_{33} (432.5 GPa) of $P2_1/m$-SiB_6 is the largest one suggesting its specially low compressibility along c-axis. Additionally, the C_{11} value of SiB_{36} reaches up to 419.3 GPa confirming its outstanding incompressibility along a-axis; meanwhile, its C_{33} is 431.5 GPa, the second highest value, predicting the excellent elastic properties of SiB_{36}.

To further demonstrate the elastic properties of Si–B crystals, bulk modulus, shear modulus, Young's modulus, Poisson's ratio and universal elastic anisotropy index (A^U) were estimated from the calculated individual elastic constants (as shown in Table 4), the previous available results are also listed for comparison and verifying the reliability of our calculation (as shown in ESI†). In general, our calculated results are in reasonable accordance with the reported data, however, it should not be ignored that the bulk moduli (181.3 GPa) of β-rh B is 11% less than the theoretical result (203.5 GPa) predicted by Masago, et al.[37] The different approximation methods may induce the deviation between the two considered values, since local-density approximation (LDA) was employed in ref. 37 while our ab initio calculation adopted GGA as the approximation method. In consideration of first-principles calculation for elastic properties (elastic constant, bulk/shear moduli, etc.), LDA results are probably larger than the actual values, on the other hand, GGA method is likely to complete tasks with underestimation, which can also explain the fact that our results are relatively smaller than the experimental data. According to Table 4, the bulk modulus (183.5 GPa) of SiB_{36} is the largest B, while SiB_6 has the largest G (153.8 GPa) and E (358.8 GPa). The intensity parameters of the other phases are just slightly lower, also indicating their comparative hardness. However, it is unexpected that the shear moduli of SiB_4 drops to 55.4 GPa, for its structure is particularly similar to SiB_3 (G = 129.8 GPa) and their bulk modulus are very close (172.1 GPa for SiB_4, 171.2 GPa for SiB_3). Comparing the two structures in Fig. 2,

Table 4 The calculated bulk modulus (B, B_V and B_R in GPa), shear modulus (G, G_V and G_R in GPa), Young's modulus (E in GPa), Poisson's ratio (ν), Pugh's ration (B/G) and universal elastic anisotropy (A^U) of Si–B system

Phase	S.G.	B	B_V	B_R	G	G_V	G_R	E	ν	B/G	A^U
SiB$_3$	$R\bar{3}m$	171.2	171.4	171.1	129.8	130.3	129.3	310.8	0.20	1.32	0.041
SiB$_4$	$R\bar{3}m$	172.1	173.4	170.7	55.4	71.1	39.6	150.0	0.35	3.11	4.00
SiB$_6$	$P2_1/m$	179.2	180.3	178.1	153.8	157.4	150.3	358.8	0.17	1.17	0.25
SiB$_6$-81	$R3m$	121.1	121.4	120.8	64.3	79.0	49.5	163.8	0.27	1.88	2.99
SiB$_{36}$	$R3m$	183.5	186.1	180.9	152.4	153.2	151.6	358.1	0.17	1.20	0.082
β-SiB$_3$	$Imma$	153.6	154.7	152.5	132.5	132.9	132.0	308.6	0.17	1.16	0.048

we infer that the additional boron atoms in SiB$_4$ lattice, contrast to SiB$_3$, are just right located long the spatial diagonal so as to disturb the original electronic division and impair the original bonding strength, that finally induce the conspicuous weakness along this direction which be responsible for the shear performance of crystals.

It could not be ignored that not only the elastic performances of $P2_1/m$-SiB$_6$ and $R3m$-SiB$_6$-81 are quite different, but also the elastic modulus of $R3m$-SiB$_6$-81 are much lower than the other Si–B compounds. After analyzing the structures in Fig. 2c and d and 4, we can conclude that the hexagonal crystal ($R3m$-SiB$_6$-81) belongs to layered-like structure based on the B$_6$ octahedron unit composed of eight boron atoms, and with silicon atoms located in interstitial spaces; however, configuration of the monoclinic one ($P2_1/m$-SiB$_6$) seems to be more complex with relative more covalent networks not only between boron atoms but also silicon ones involved, which avoiding layers' sliding in the lattice structure of $R3m$-SiB$_6$-81 and providing $P2_1/m$-SiB$_6$ stronger elastic properties.

The above few fluctuations can't impede us to find these general trends that both the bulk and shear modulus decreased gradually with the increasing Si concentration. Those are possibly induced by that B–B bond distance ranges are lengthened from 1.67–1.92 Å in monatomic boron to 1.84–2.04 Å so as to weaken the bond strength, in addition to the balance of electron distribution is broken and the new Si–Si, Si–B bonds are inferior to B–B bonds in hardness, contributed by the incorporation of Si atoms into the stable structure bonded by B atoms.

The ratio between the shear and bulk modulus (B/G) has been proposed by Pugh[54] to predict brittle or ductile behavior of materials. According to the Pugh criterion, a high B/G value indicates a tendency for ductility, while a low B/G value is associated with brittleness. From Table 4, SiB$_4$ (2.80), SiB$_6$-81 (1.88) are recognized with B/G value larger than the critical value (1.75) suggesting their ductile behaviors, while the other phases are expected to perform brittleness. The elastic anisotropy index (A^U) represents a universal measure to quantify the single crystal elastic anisotropy. As shown in Table 4, SiB$_3$ is the relatively most isotropic phase, with the lowest A^U value (0.041) in the whole Si–B system, contrarily, SiB$_4$ ($A^U = 4.00$) is predicted as most anisotropy crystal.

3.3. Electronic properties

The total and partial density of states (DOS) for the Si–B crystals are displayed in Fig. 5. Analyzing all the DOS patterns, we found that there are three phases: $P2_1/m$-SiB$_6$, $R3m$-SiB$_6$-81 and β-SiB$_3$ showing the semiconducting features. Incorporated with the calculated band structures of those 3 compounds (shown in Fig. 6), we collected the indirect band gaps for $P2_1/m$-SiB$_6$ and β-SiB$_3$ with energy values (eV): 0.41 and 1.461; direct band gaps for $R3m$-SiB$_6$-81 (1.654 eV), respectively. The calculated result of β-SiB$_3$ is in good accordance with the previously work[16] which showed an indirect band gap of ~1.5 eV from theoretical calculations and 2.0 eV optically determined, in addition, our calculated band gaps of α-rh B (1.533 eV) and γ-B$_{28}$ (1.580 eV) in ESI† are in good agreement with previously theoretical results:
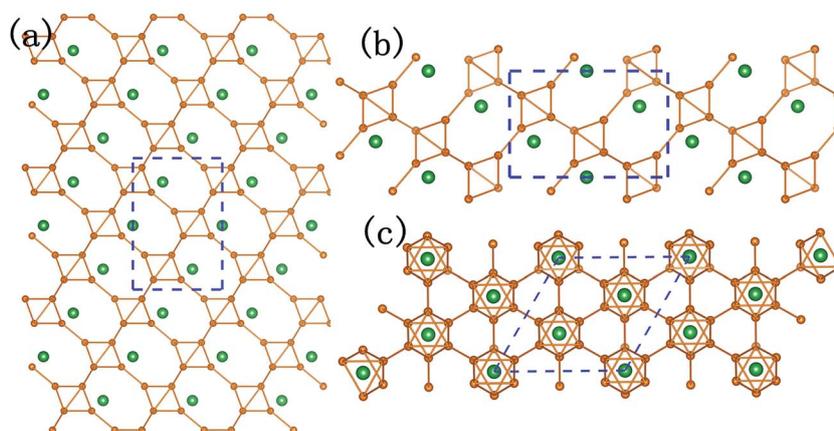
Fig. 4 Crystal structure of hexagonal SiB$_6$-81. (a), (b) and (c) are along a-, b- and c-axis, respectively.
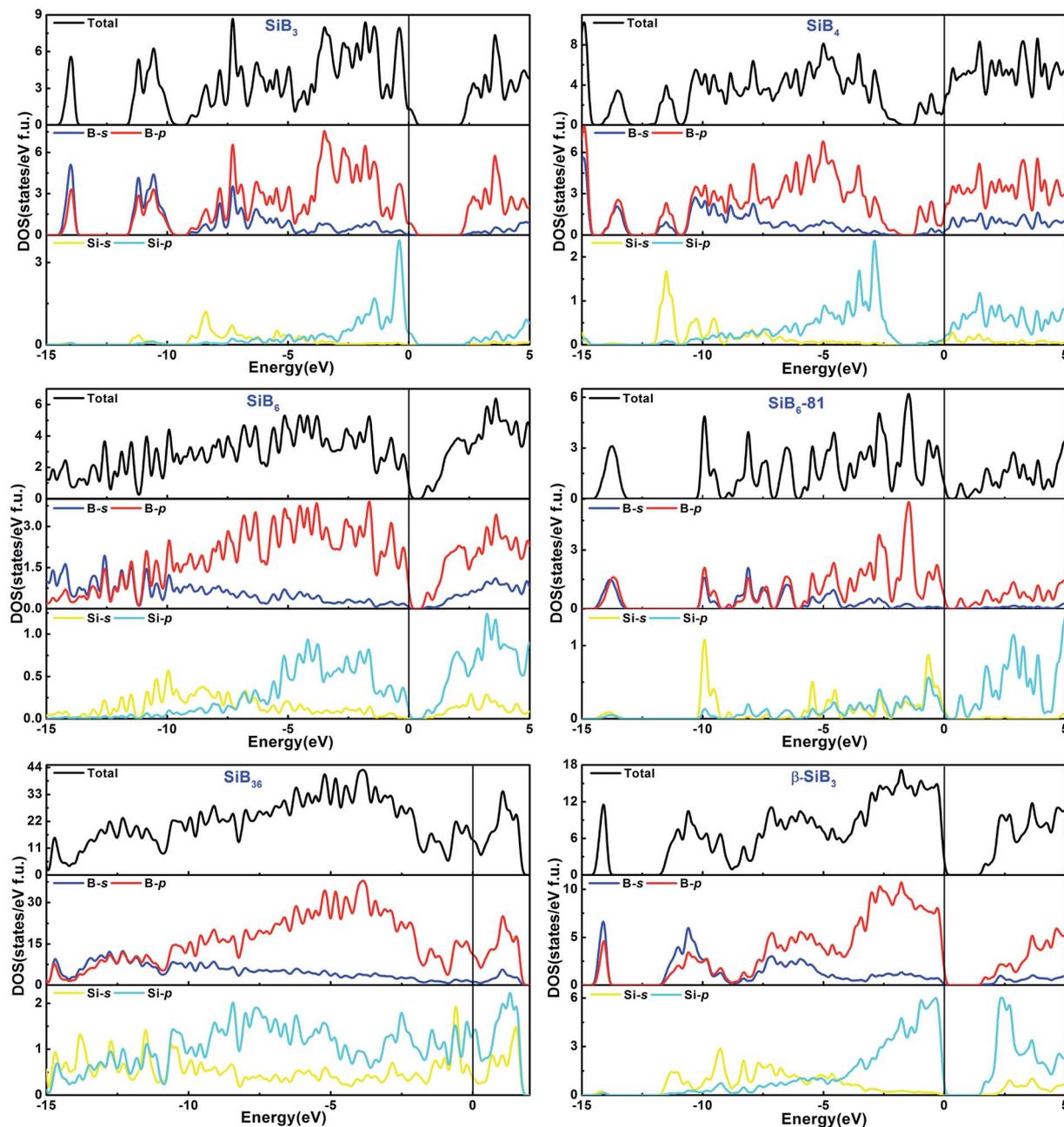
Fig. 5 Calculated total and partial density of states of phases in Si−B system. Fermi energy level is indicated by a vertical line.

1.54 eV (ref. 25) and 1.7 eV,[55] therefore our calculation of electronic properties is dependable. The estimated band gap of SiB_6 by Feigelson and Kingery is about 1.2 eV (ref. 56) and our calculated value is 0.41 eV. Since the general tendency is allowed that the generalized gradient approximation gives narrower band gap than the observed one, the estimated value seems to be reasonable. The temperature dependence of the electrical conductivity of SiB_3 was measured in ref. 56 and it was concluded that SiB_3 is a semiconductor with the energy gap of 1.2 eV, which does not agree to the present work. We infer that the increase in electric conductivity with the temperature observed by Feigelson and Kingery[56] is due to the rising hopping probability of the localized state at higher temperature, which is possibly induced by disordered arrangement of the atoms, but due to the semiconducting band conduction. $R3m$-SiB_6-81 has a wide band gap of 1.654 eV, this new theoretically suggested material might be useful as a refractory n-type semiconductor capable of operating in extreme environments, so the results reported herein warrant future investigations of synthesizing this Si–B compound.

Since it is widely accepted that the DFT-GGA approximation probably underestimates the band gap of solids,[24,32] DFT-LDA approximation was also applied to study the electronic structures and verify the GGA calculation results. The LDA
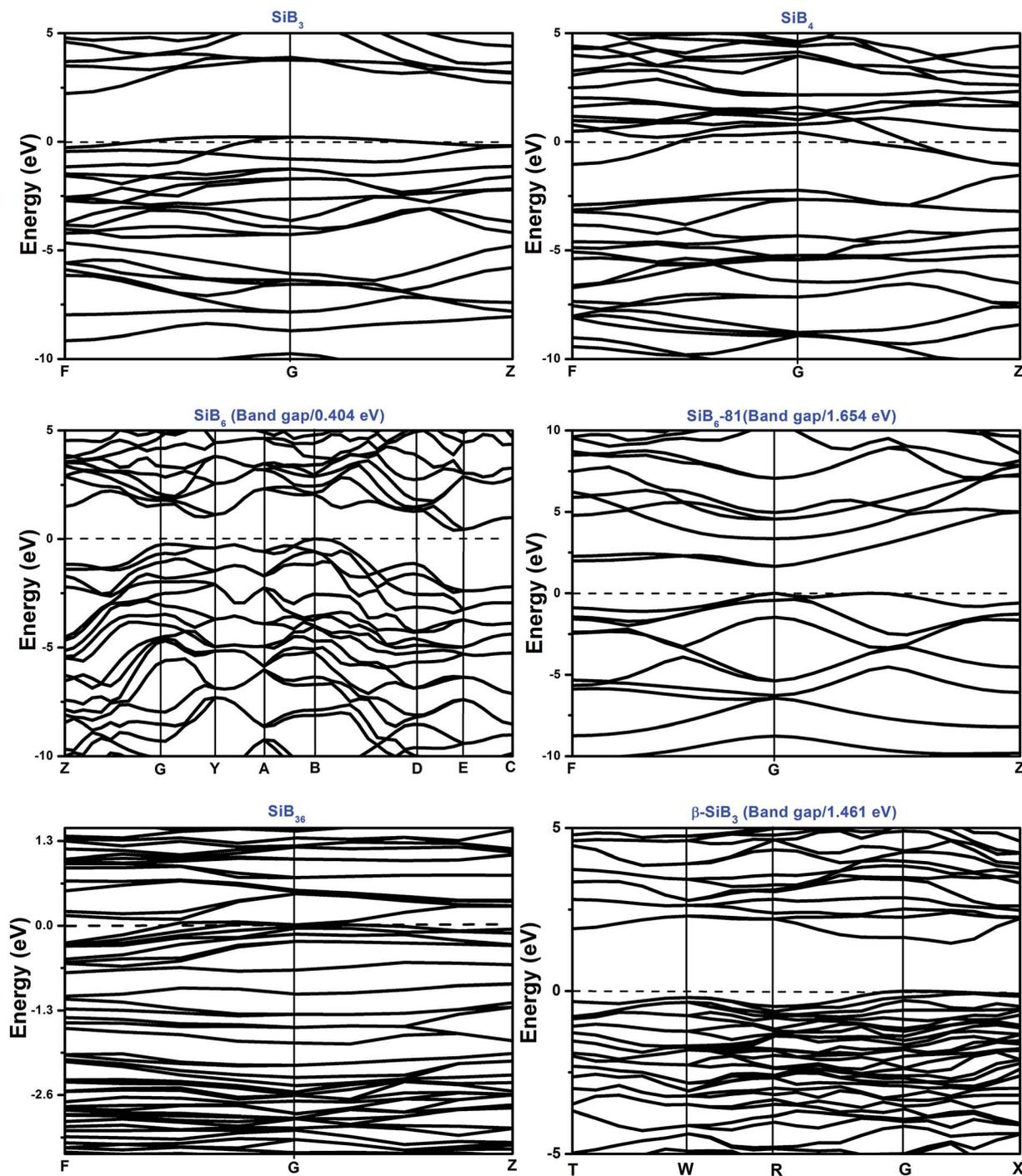
Fig. 6 Calculated band structures of Si−B phases. Fermi energy level is indicated by a dotted line.

calculation results indicate that the band gaps are 0.371 eV, 1.621 eV and 1.502 eV for SiB_6, SiB_6-81 and β-SiB_3, respectively. Those reasonable differences between GGA and LDA calculations solidify our conclusions in electronic properties research. The DOS and band structures results from DFT-LDA calculations are available in ESI.†

There is no band gap provided by band structures of SiB_4 and SiB_{36} in Fig. 6, as well as their DOS values are relatively large at Fermi level, indicating they are energetically unstable under 0 K

and GPa. It can be found that there is a wide overlap between B-*s* state and B-*p* state of SiB_3, SiB_4, SiB_6, SiB_6-81, SiB_{36} and β-SiB_3 from −14 eV to −5 eV, respectively, demonstrating the strong sp³ hybridization of covalent bonds, which mainly accounts for their relatively good performances in bulk modulus. It is interesting to notice that for SiB_3 and SiB_4, there are two sharp peaks in both sides of the Fermi level and DOS between the peaks are not 0 eV, which implying pseudogap exists in both of these two phases. Those pseudogap valleys show stronger

covalent interaction in the structures. Moreover, there is a general feature for the Si–B binaries that below the Fermi level, the valence bands were dominated by B states with both B-s and B-p states at lower band while B-p states at higher band. Nevertheless, as shown in Fig. 5, the contributions to the total DOS of Si–B compounds from the Si states are not significant because Si atoms donate electrons to B–B network to stabilize the structure, for example, about 0.96 electron transformed from one Si atom to B–B network for SiB_6 by analyzing the atomic Mulliken overlap populations.

In addition to the calculated values of two indirect band gaps and one direct band gap, in the band structures of these six Si–B binaries (shown in Fig. 6), it can also be noticed that the distributions of band structures of $P2_1/m$-SiB_6, SiB_{36} and β-SiB_3 are more concentrated than those of the other three phases; and each energy band at different points fluctuates less drastically. Those details account for that electron localizations of the energy bands of SiB_6, SiB_{36} and β-SiB_3 are more intensive and effective mass of an electron is relatively larger; in contrast, energy bands of SiB_3, SiB_4 and $R3m$-SiB_6-81 display more electron nonlocality.

4. Conclusions

We systematically investigated the crystal structures, phase stability, mechanical properties and electronic structures of silicon–boron system by using first-principles calculations of density functional theory. Previously suggested phase: $Pm\bar{3}m$-SiB_6 is found to be mechanically unstable, and the new structure of $P2_1/m$-SiB_6 is proposed in this paper. Another new structure of SiB_{36} is suggested, in which two layers constituted with B_{80} unit are connected by two neighbor parallel B_6 layers, in addition to be covalently bound through junctional atom B_{15} while Si atoms are partially located at interstitial sites in the space surrounded by the joint B_6 layers. We find the general trends that both the bulk and shear modulus decreased gradually with the increasing Si concentration, because the introduced Si–Si and Si–B bonds are weaker than the original B–B network. Although the elastic properties of β-SiB_3 are slightly inferior to α-SiB_3, its wide band gap (1.461 eV) makes β-SiB_3 a potential p-type semiconductor. In addition to β-SiB_3, $P2_1/m$-SiB_6 is found to be with an indirect band gap of 0.41 eV; while $R3m$-SiB_6-81 has a direct band gap of 1.654 eV, this new theoretically suggested material might be useful as a refractory n-type semiconductor capable of operating in extreme environments that deserving more efforts in research of this Si–B compound.

References

1 R. Riedel, *Adv. Mater.*, 1994, **6**, 549–560.

2 *Mechanical properties and their relation to microstructure*, D. Sherman and D. Brandon, Wiley-VCH Verlag GmbH, Weinheim, Germany, 2000.

3 C. Wood, *Mater. Res. Soc. Symp. Proc.*, 1987, **97**, 335–346.

4 J.-M. Darolles, T. Lepetre and J.-M. Dusseau, *Phys. Status Solidi A*, 1980, **58**, K71–K75.

5 M. Mukaida, T. Tsunoda, M. Ueda and Y. Imai, *Proc. 19th Int. Conf. Thermoelectrics*, 2000, p. 255.

6 J. Wu, W. Ma, D. Tang, B. Jia, B. Yang, D. Liu and Y. Dai, *Procedia Eng.*, 2012, **31**, 297–301.

7 Y. Imai, M. Mukaida, M. Ueda and A. Watanabe, *J. Alloys Compd.*, 2002, **347**, 244–251.

8 C. Brosset and B. Magnusson, *Nature*, 1960, **187**, 54–55.

9 V. I. Matkovich, *Acta Crystallogr.*, 1960, **13**, 679–680.

10 H. F. Rizzo and L. R. Bidwell, *J. Am. Ceram. Soc.*, 1960, **43**, 550–552.

11 B. Magnusson and C. Brosset, *Acta Chem. Scand.*, 1962, **16**, 449–455.

12 On refractory boron compounds crystallizing in B_4C-type structures, ed. T. Lundstrom and H. Bolmgren, *Jpn. J. Appl. Phys. Ser.*, 1994, vol. 10, pp. 1–4.

13 E. Colton, *J. Am. Chem. Soc.*, 1960, **82**, 1002.

14 C. F. Cline and D. E. Sands, *Nature*, 1960, **185**, 456.

15 R. Tremblay and R. Angers, *Ceram. Int.*, 1989, **15**, 73–78.

16 J. R. Salvador, D. Bilc, S. D. Mahanti and M. G. Kanatzidis, *Angew. Chem.*, 2003, **115**, 1973–1976.

17 T. L. Aselage, *J. Mater. Res.*, 1998, **13**, 1786–1794.

18 T. L. Aselage and D. R. Tallant, *Phys. Rev. B: Condens. Matter Mater. Phys.*, 1998, **57**, 2675–2678.

19 N. N. Zhuravlev, *Kristallografiya*, 1956, **1**, 666–668.

20 M. Vlasse, G. A. Slack, M. Garbauskas, J. S. Kasper and J. C. Viala, *J. Solid State Chem.*, 1986, **63**, 31–45.

21 R. F. Giese, J. Economy and V. I. Matkovich, *Z. Kristallogr.*, 1965, **122**, 144–147.

22 B. Armas, G. Male, D. Salanoubat, C. Chatillon and M. Allibert, *J. Less-Common Met.*, 1981, **82**, 245–254.

23 T. B. Massalski, H. Okamoto, P. R. Subramanian and L. Kacprzak, *Binary alloy phases diagrams*, ASM, Materials Park, OH, 2nd edn, 1990.

24 T. Ogitsu, E. Schwegler and G. Galli, *Chem. Rev.*, 2013, **113**, 3425–3449.

25 B. Albert and H. Hillebrecht, *Angew. Chem., Int. Ed.*, 2009, **48**, 8640–8668.

26 B. Callmer, *Acta Crystallogr., Sect. B: Struct. Crystallogr. Cryst. Chem.*, 1977, **33**, 1951–1954.

27 D. L. V. K. Prasad, M. M. Balakrishnarajan and E. D. Jemmis, *Phys. Rev. B: Condens. Matter Mater. Phys.*, 2005, **72**, 195102.

28 T. Ogitsu, F. Gygi, J. Reed and Y. Motome, *J. Am. Chem. Soc.*, 2009, **131**, 1903–1909.

29 S. Shang, Y. Wang, R. Arroyave and Z. K. Liu, *Phys. Rev. B: Condens. Matter Mater. Phys.*, 2007, **75**, 092101.

30 S. Lee, D. Bylander, S. Kim and L. Kleinman, *Phys. Rev. B: Condens. Matter Mater. Phys.*, 1992, **45**, 3248–3251.

31 W. Hayami and S. Otani, *J. Solid State Chem.*, 2010, **183**, 1521–1528.

32 S. Aydin and M. Simsek, *J. Alloys Compd.*, 2011, **509**, 5219–5229.

33 J. L. Hoard, R. E. Hughes and D. E. Sands, *J. Am. Chem. Soc.*, 1958, **80**, 4507–4515.

34 G. Will and K. Ploog, *Nature*, 1974, **251**, 406–408.

35 W. Hayami and S. Otani, *J. Phys. Chem. C*, 2007, **111**, 10394–10397.

36 D. Li, Y. N. Xu and W. Y. Ching, *Phys. Rev. B: Condens. Matter Mater. Phys.*, 1992, **45**, 5895–5905.

37 A. Masago, K. Shirai and H. Katayama-Yoshida, *Phys. Rev. B: Condens. Matter Mater. Phys.*, 2006, **73**, 104102.

38 M. A. White, A. B. Cerqueira, C. A. Whitman, M. B. Johnson and T. Ogitsu, *Angew. Chem., Int. Ed.*, 2015, **54**, 3626–3629.

39 P. J. D. L. M. D Segall, M. J Probert, C. J Pickard, P. J Hasnip, S. J Clark and M. C Payne, *J. Phys.: Condens. Matter*, 2002, **14**, 2717–2744.

40 J. P. Perdew, J. A. Chevary, S. H. Vosko, K. A. Jackson, M. R. Pederson, D. J. Singh and C. Fiolhais, *Phys. Rev. B: Condens. Matter Mater. Phys.*, 1992, **46**, 6671–6687.

41 J. P. Perdew, K. Burke and M. Ernzerhof, *Phys. Rev. Lett.*, 1996, **77**, 3865–3868.

42 R. Hill, *Proc. Phys. Soc.*, 1952, **65**, 349–354.

43 S. I. Ranganathan and M. Ostoja-Starzewski, *Phys. Rev. Lett.*, 2008, **101**, 055504.

44 M. Born and K. Huang, *Dynamical theory of crystal lattices*, Oxford University Press, Oxford, 1954.

45 J. F. Nye, *Physical properties of crystals*, Oxford University Press, Oxford, 1985.

46 Y. Wang, J. Lv, L. Zhu and Y. Ma, *Phys. Rev. B: Condens. Matter Mater. Phys.*, 2010, **82**, 094116.

47 Y. Wang, J. Lv, L. Zhu and Y. Ma, *Comput. Phys. Commun.*, 2012, **183**, 2063–2070.

48 C. F. Cline, *J. Electrochem. Soc.*, 1959, **106**, 322–325.

49 JCPDS pattern #35-777, International Centre for Diffraction Data, Newton Square, PA.

50 A. I. Zaitsev and A. A. Kodentsov, *J. Phase Equilib.*, 2001, **22**, 126–135.

51 R. W. Olesinski and G. J. Abbaschian, *Bull. Alloy Phase Diagrams*, 1984, **5**, 478–484.

52 B. G. Arabey, *Izv. Akad. Nauk SSSR, Neorg. Mater.*, 1979, **15**, 1589–1592.

53 J. Roger, V. Babizhetskyy, J.-F. Halet and R. Guérin, *J. Solid State Chem.*, 2004, **177**, 4167–4174.

54 S. F. Pugh, *Philos. Mag.*, 1954, **45**(7), 823–843.

55 E. Zarechnaya, L. Dubrovinsky, N. Dubrovinskaia, Y. Filinchuk, D. Chernyshov, V. Dmitriev, N. Miyajima, A. El Goresy, H. Braun, S. Van Smaalen, I. Kantor, A. Kantor, V. Prakapenka, M. Hanfland, A. Mikhaylushkin, I. Abrikosov and S. Simak, *Phys. Rev. Lett.*, 2009, **102**, 185501.

56 R. S. Feigelson and W. D. Kingery, *Ceram. Bull.*, 1963, **42**, 688.